An x-ray diffraction and magnetic susceptibility study of $Yb_xY_{2-x}O_3$

J. Phys.: Condens. Matter **9** (1997) 4103–4111. Printed in the UK PII: S0953-8984(97)80226-3

An x-ray diffraction and magnetic susceptibility study of $Yb_xY_{2-x}O_3$

M Mitric†, B Antic†, M Balanda‡, D Rodic† and M Lj Napijalo§

† 'Vinča' Institute of Nuclear Sciences, Laboratory of Solid State Physics, PO Box 522, 11001 Belgrade, Yugoslavia

‡ Institute of Nuclear Physics, Radzikowskiego 152, 31-342 Krakow, Poland

§ Faculty of Physics, University of Belgrade, PO Box 368, 11001 Belgrade, Yugoslavia

Received 10 December 1996

Abstract. Polycrystalline samples of the new semimagnetic semiconductor $Yb_xY_{2-x}O_3$ (x = 0.06, 0.12, 0.25, 0.39, 1.00, 1.40, 1.80) were obtained by ceramic technology. An x-ray diffraction experiment was performed on all of the samples at room temperature. These data provided the basis for Rietveld refinements. The refinements showed that Yb^{3+} ions preferentially occupy the 24d position. The lattice constants and the mean cation–anion distances decrease linearly with the Yb^{3+}-ion concentration. The inverse magnetic susceptibilities for all of the samples depend linearly on the temperature for 4 K $< T <$ 30 K. In this region only the lowest Kramer's doublet is populated, and for that level the effective magnetic quantum number M_{1eff} is deduced. The Curie–Weiss paramagnetic temperatures $\theta(x)$ obtained from the low-temperature region depend linearly on the concentration x. Over the whole experimental region 4 K $< T <$ 250 K, the magnetic susceptibility deviates from the Curie–Weiss law, and its calculation requires inclusion of the first excited Kramer's doublet. The effective magnetic quantum number M_{2eff} and energy gap ΔW of the first excited doublet were deduced.

1. Introduction

In this paper we have studied the structure and magnetic properties of the $Yb_xY_{2-x}O_3$ solid solutions. The mixed rare-earth–yttrium sesquioxides $RE_xY_{2-x}O_3$ are a new class of diluted magnetics. Some of them were recently synthesized and studied [1–4]. The structure and magnetic properties of all of the $RE_xY_{2-x}O_3$ compounds have not yet been completely investigated. The $Yb_xY_{2-x}O_3$ compounds are of special interest due to the presence of Yb^{3+} ions, which are the last in the lanthanide series with unfilled f shells. The free Yb^{3+} ion has the configuration $4f^{13}$ which gives rise to a $J = 7/2$ ground manifold and a $J = 5/2$ excited manifold at about 10 000 cm^{-1}. Of the splittings of all of the rare-earth ions, these splittings for Yb^{3+} are the largest, and hence the excited manifold $J = 5/2$ does not significantly contribute to the magnetic properties. On the other hand, the crystal-field splitting of the $J = 7/2$ ground manifold of the Yb^{3+} ion should be included in considerations of the magnetic properties of $Yb_xY_{2-x}O_3$ compounds in our experimental region 4 K $< T <$ 250 K.

The investigation of the crystal structure provides a basis for an understanding of the magnetic properties of the Yb^{3+} ion in $Yb_xY_{2-x}O_3$. The crystal structures of the constitutive compounds Y_2O_3 and Yb_2O_3 are well known. Both oxides crystallize in the bixbyite structure in the space group $Ia3$. In this space group, cations occupy the special positions 8b and 24d [5] with local symmetries C_{3i} and C_2, respectively. The position 24d has one

0953-8984/97/204103+09$19.50

degree of freedom. The cations in both positions are octahedrally surrounded by oxygen ions. The oxygen ion in the general 48e position is surrounded by four cations [5].

From the magnetic point of view, Y_2O_3 is diamagnetic, whereas Yb_2O_3 exhibits antiferromagnetic non-collinear structure below $T_N = 2.3$ K [6]. Yb^{3+} ions in 8b positions have magnetic moments directed along the [111] direction but not along the particular [111] local symmetry axis [6]. The magnetic moments of Yb^{3+} ions in 24d positions point along the [110] direction [6]. Sites related by body-centre translations have their moments directed oppositely [6]. Neutron measurements indicated different magnetic moments at 24d and 8b crystallographic sites [6]. In the paramagnetic phase, in the temperature range $4\ \text{K} < T < 250\ \text{K}$, the inverse susceptibility of Yb_2O_3 is non-linear versus temperature, and does not obey the Curie–Weiss law [7, 8].

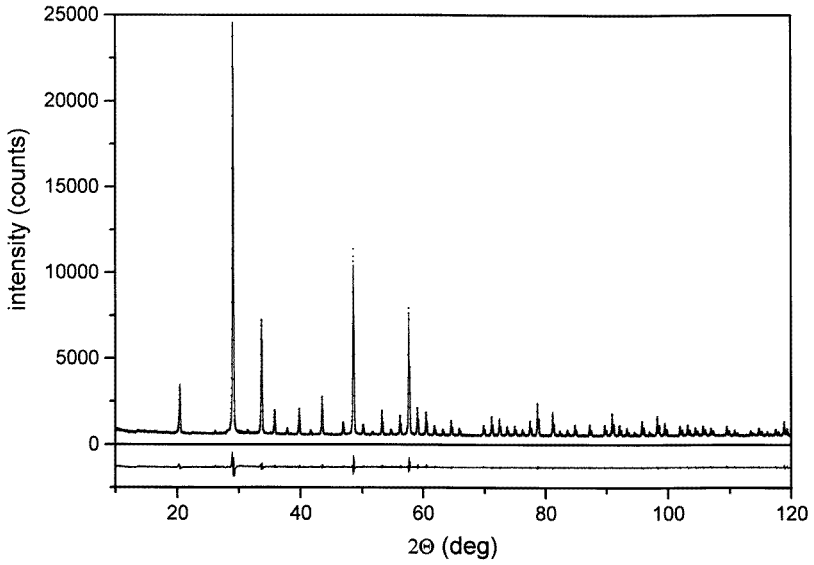

Figure 1. The final Rietveld plot for $Yb_{0.25}Y_{1.75}O_3$. The dots represent experimental points, and the full line represents the calculation. The difference of the experimental and calculated values is given at the bottom.

2. Experimental procedure

Polycrystalline samples of $Yb_xY_{2-x}O_3$ ($x = 0.06$, 0.12, 0.25, 0.39, 1.00, 1.40, 1.80) were obtained by ceramic technology. The starting oxides Y_2O_3 (purity 99.99%) and Yb_2O_3 (purity 99.95%) were mixed in the appropriate stoichiometric ratios. The mixtures were dissolved in hot concentrated HNO_3. The nitrates obtained were coprecipitated and simultaneously mixed in concentrated ammonium hydroxide. In this way the best mixing and lower firing temperatures were achieved. The hydroxides obtained were fired at 1300 °C for 48 hours. In order to obtain higher x-ray densities the samples were reground, thoroughly mechanically mixed, pressed at 130 MPa, and refired at 1400 °C for several days. The firing was followed by slow cooling.

The x-ray powder diffraction data were collected, at room temperature, on a Phillips PW 1010 powder diffractometer with a position-sensitive detector and Ni-filtered Cu Kα_1, α_2

radiation. The data were collected in the 2θ region 10–120°, with a step length of 0.02° and an exposure time of 10 s per step.

The absolute magnetic measurements were made on a LakeShore Series 7000 DC magnetometer. The temperature range was from 4 K to 250 K. The applied field was 1.0 T.

3. The refinement of the crystal structure

The crystal structures of the compounds $Yb_xY_{2-x}O_3$ were refined by the Rietveld profile method, using the program version DBWS-9006 [9]. The starting atomic and crystal parameters for the refinement process were taken from [10]. These solid solutions are ionic crystals, and the intensity data were evaluated assuming ionic scattering curves for the cations [11] and oxygen ions [12] (the data for the refinement are weakly sensitive to the choice of ionic or atomic scattering factors). A pseudo-Voigt peak shape was assumed in the refinements. The final Rietveld plot for $Yb_{0.25}Y_{1.75}O_3$ is shown in figure 1.

Table 1. Refined values of the atomic parameters for $Yb_xY_{2-x}O_3$.

x:		0.06	0.12	0.25	0.39
O(48e)	x (Å)	0.3889(7)	0.3906(7)	0.3914(6)	0.3904(7)
	y (Å)	0.1537(6)	0.1538(6)	0.1536(6)	0.1532(6)
	z (Å)	0.3796(8)	0.3796(8)	0.3811(7)	0.3802(8)
Yb, Y(24d)	x (Å)	−0.0325(1)	−0.0327(1)	−0.327(1)	−0.0325(1)
Y(8b)	N	0.995(16)	0.953(15)	0.907(12)	0.830(14)
Yb(8b)	N	0.005(16)	0.047(15)	0.093(12)	0.170)14)
Y(24d)	N	2.885(16)	2.807(15)	2.592(12)	2.370(14)
Yb(24d)	N	0.115(16)	0.193(15)	0.408(12)	0.630(14)
24d	B (Å^2)	0.13(10)	0.17(8)	0.30(6)	0.31(6)
8b	B (Å^2)	0.11(10)	0.30(4)	0.27(3)	0.33(3)
48e	B (Å^2)	0.27(14)	0.37(14)	0.65(12)	0.74(13)
	a (Å)	10.5924(1)	10.5883(1)	10.5770(1)	10.5645(1)
x:		1.00	1.40	1.80	2
O(48e)	x (Å)	0.3897(6)	0.3926(11)	0.3911(9)	0.3903(6)
	y (Å)	0.1541(6)	0.1515(9)	0.1540(9)	0.1515(6)
	z (Å)	0.3798(7)	0.3814(10)	0.3810(10)	0.3824(7)
Yb, Y(24d)	x (Å)	−0.0326(1)	−0.0327(1)	−0.0328(1)	−0.0331(1)
Y(8b)	N	0.540(12)	0.326(21)	0.167(18)	0
Yb(8b)	N	0.460(12)	0.674(21)	0.833(18)	1
Y(24d)	N	1.460(12)	0.874(21)	0.233(18)	0
Yb(24d)	N	1.540(12)	2.126(21)	2.767(18)	3
24d	B (Å^2)	0.26(4)	0.24(7)	0.07(5)	0.20(4)
8b	B (Å^2)	0.22(3)	0.15(3)	0.14(2)	0.12(2)
48e	B (Å^2)	0.72(13)	0.73(19)	0.28(18)	0.34(12)
	a (Å)	10.5151(1)	10.4807(1)	10.4470(1)	10.4304(1)

The last cycles of the refinements were made by varying 22 parameters: one parameter for the scale factor, one zero point, three halfwidths, one mixing, one preference, one asymmetry, five parameters for the description of the background, and one lattice constant parameter. The remaining eight atomic parameters were: the x-coordinate for the cation in a 24d position, three oxygen coordinates, three B-factors for three different crystallographic positions, and one occupation number. The occupancy of ytterbium in position 8b was

refined while coupled with the occupancy of yttrium at the same site, and the occupancies of ytterbium and yttrium at 24d positions, in order to keep the stoichiometric ratio constant. The final refinement for Yb_2O_3 was done with 21 parameters. The crystal data and atomic parameters from the least-squares refinements are given in table 1.

The coefficients of the cationic distribution K, calculated from the equation

$$K = \frac{N_{Yb}(8b)}{N_Y(8b)} \frac{N_Y(24d)}{N_{Yb}(24d)} \tag{1}$$

(N_{Yb} (8b) and N_{Yb} (24d) represent the occupancies of the Yb^{3+} ions at 8b and 24d positions, respectively; N_Y (8b) and N_Y (24d) represent the occupancies of the Y^{3+} ions at 8b and 24d positions, respectively) are 0.13(42), 0.72(30), 0.65(12), 0.77(10), 0.80(5), 0.85(11), and 0.42(9) for the samples with $x = 0.06$, 0.12, 0.25, 0.39, 1.00, 1.40, and 1.80, respectively. If K is close to 1, the cationic distribution is random. The values of the coefficient K show that in all of the samples, Yb^{3+} ions preferentially occupy 24d positions.

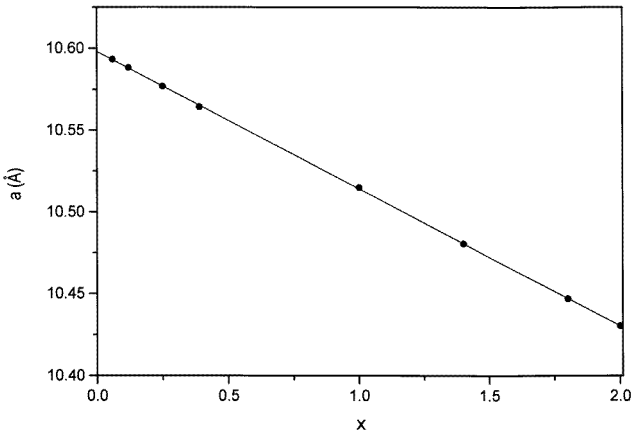

Figure 2. Vegard's rule for $Yb_xY_{2-x}O_3$ solid solutions.

The lattice constants of $Yb_xY_{2-y}O_3$ decrease with the increase of the Yb concentration obeying Vegard's rule (figure 2):

$$a = a_0 + a_1x \tag{2}$$

where $a_0 = 10.5978(2)$ Å corresponds to Y_2O_3 and $a_1 = -0.0837(2)$ Å corresponds to the difference of the ionic radii $r(Yb^{3+}) = 0.858$ Å and $r(Y^{3+}) = 0.892$ Å [13].

The B-factors are similar for cations in the two crystallographic positions (table 1), and smaller than the B-factor for the lighter oxygen ion, as expected. The B-factors are generally bigger for medium concentrations.

The mean cation–anion distance (table 2) linearly decreases with the increase of the Yb^{3+} concentration, obeying the rule

$$d = d_0 + d_1x \tag{3}$$

where $d_0 = 2.283(1)$ Å and $d_1 = -0.0175(2)$ Å. The concentration dependencies of individual cation–anion distances are not linear.

Table 2. The nearest cation–anion distances for $Yb_xY_{2-x}O_3$.

x:	0.06	0.12	0.25	0.39	1.00	1.40	1.80	2
Yb, Y(8b)–O (Å)	2.263(7)	2.266(7)	2.280(6)	2.267(7)	2.244(6)	2.280(10)	2.248(9)	2.244(8)
Yb, Y(24d)–O (Å)	2.340(7)	2.342(7)	2.335(7)	2.320(7)	2.321(6)	2.308(10)	2.307(9)	2.303(8)
Yb, Y(24d)–O (Å)	2.283(7)	2.279(7)	2.282(6)	2.275(7)	2.271(6)	2.243(10)	2.257(9)	2.253(8)
Yb, Y(24d)–O (Å)	2.241(7)	2.238(7)	2.220(6)	2.231(7)	2.223(6)	2.202(10)	2.194(9)	2.191(8)
Mean distance (Å)	2.282(7)	2.281(7)	2.279(6)	2.276(7)	2.265(6)	2.258(10)	2.252(9)	2.248(8)

4. The magnetic susceptibility

The experimentally obtained magnetic susceptibility is the sum of paramagnetic and diamagnetic susceptibilities. To obtain the paramagnetic susceptibilities, the diamagnetic contributions of the Y^{3+}, Yb^{3+}, and O^{2-} ions [14] were subtracted from the experimental data.

The temperature dependences of the inverse paramagnetic susceptibilities of the $Yb_xY_{2-x}O_3$ samples can be divided in two regions. In the low-temperature region, for $T \lesssim 30$ K, the inverse paramagnetic susceptibilities depend linearly on temperature (see figures 3(a), 3(b)). However, in the high-temperature region, for $T > 30$ K, the inverse paramagnetic susceptibilities are non-linear versus temperature (see figures 4(a), 4(b)). This deviation from the Curie–Weiss behaviour reflects the splitting of the Yb^{3+}-ion ground state under the influence of the crystal field. In the crystal fields of C_2 and C_{3i} symmetry, corresponding to the crystallographic positions 24d and 8b, respectively, the eightfold ground level $^2F_{7/2}$ of the Yb^{3+} ions splits into four Kramer's doublets [15–17]. Each doublet can be characterized by the effective magnetic quantum number $\pm M_{i\,eff}$ ($i = 1$, 2, 3, and 4). The values of the effective magnetic quantum number of each sublevel should be obtained as a linear combination of the magnetic quantum numbers of the free ion. Note that $M_{i\,eff}$ for a given value of i is different for the crystallographic positions 24d and 8b due to the different crystal-field symmetries. From our experiment, we can deduce only a weighted-average value of the magnetic quantum numbers $M_{i\,eff}$(24d) and $M_{i\,eff}$(8b), and in the rest of this paper $M_{i\,eff}$ denotes this value.

Table 3. The magnetic moments of the lowest and the first excited Kramer's doublets, and the energy gap between them.

x:	0.06	0.12	0.25	0.39	1.00	1.40	1.80	2
M_{1eff}	1.75(12)	1.66(12)	1.66(6)	1.72(6)	1.70(3)	1.67(3)	1.70(3)	1.71(1)
M_{2eff}	1.99(12)	2.33(10)	2.48(8)	2.44(8)	2.57(6)	2.52(6)	2.61(6)	2.60(3)
$\Delta W/k_B$ (K)	85(12)	168(9)	179(8)	166(8)	205(8)	191(7)	221(6)	225(5)
C_M/x (emu K/g-ion)	1.50(2)	1.35(2)	1.35(2)	1.46(2)	1.41(1)	1.41(1)	1.42(1)	1.44(1)

In the temperature range of our experiments the population of the Kramer's doublets varies, and the effective moment becomes temperature dependent. However, in the low-temperature region ($T < 30$ K) only the lowest Kramer's doublet of Yb^{3+} ions is populated [18], and the effective magnetic moment corresponds to this doublet. Consequently, in this region, the paramagnetic susceptibilities can be fitted to the Curie–Weiss law:

$$\chi_M = \frac{C_M}{T - \theta}. \tag{4}$$

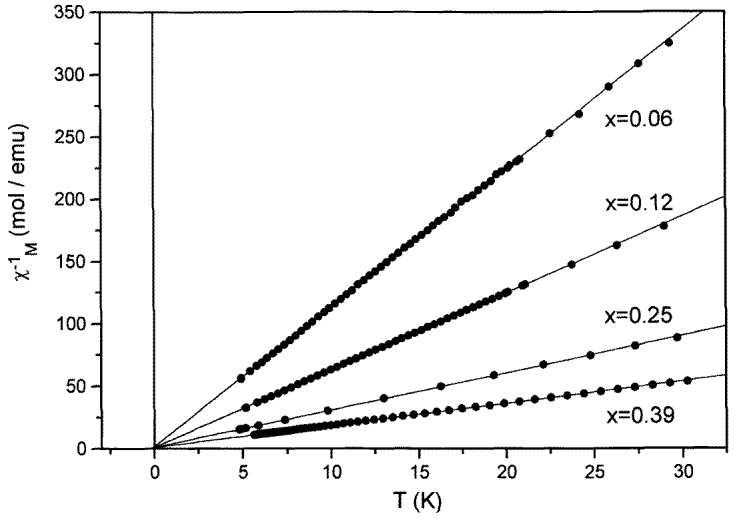

(a)

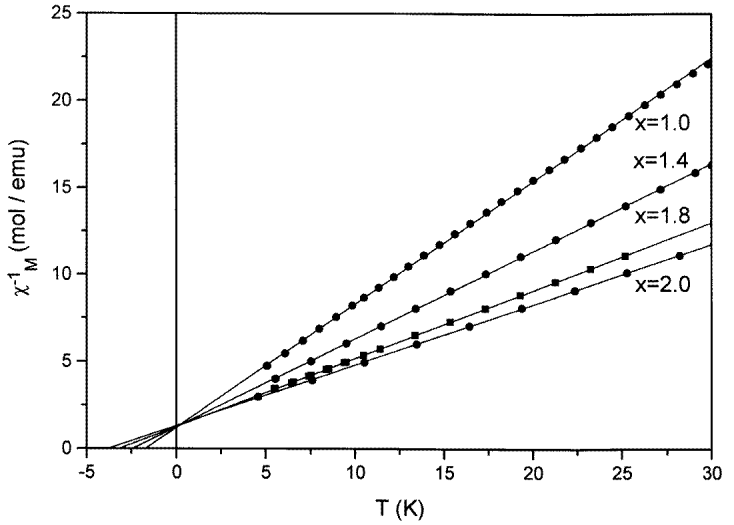

(b)

Figure 3. The inverse low-temperature susceptibilities for $Yb_xY_{2-x}O_3$ samples. The dots represent experimental points, and the full lines represent the calculation.

where C_M denotes the molar Curie constant $C_M = xN_{Av}g_J^2\mu_B^2M_{1eff}^2/k_B$, where x denotes the concentration, N_{Av} is Avogadro's number, $g_J = 8/7$ is Landé's splitting factor, μ_B is the Bohr magneton, M_{1eff} is the effective magnetic quantum number of the lowest Kramer's doublet of Yb^{3+} ions, k_B is the Boltzmann constant, and θ is the Curie–Weiss paramagnetic temperature. In equation (4) the Van Vleck contribution is neglected, because the first excited level $^2F_{5/2}$ of the free Yb^{3+} ion lies at about 10 300 cm^{-1} [16]. The values obtained for M_{1eff} and C_M/x, which corresponds to the gram-ion Curie constant of the Yb^{3+} ion, versus concentration are listed in table 3. All of the values of C_M/x are smaller than the Curie

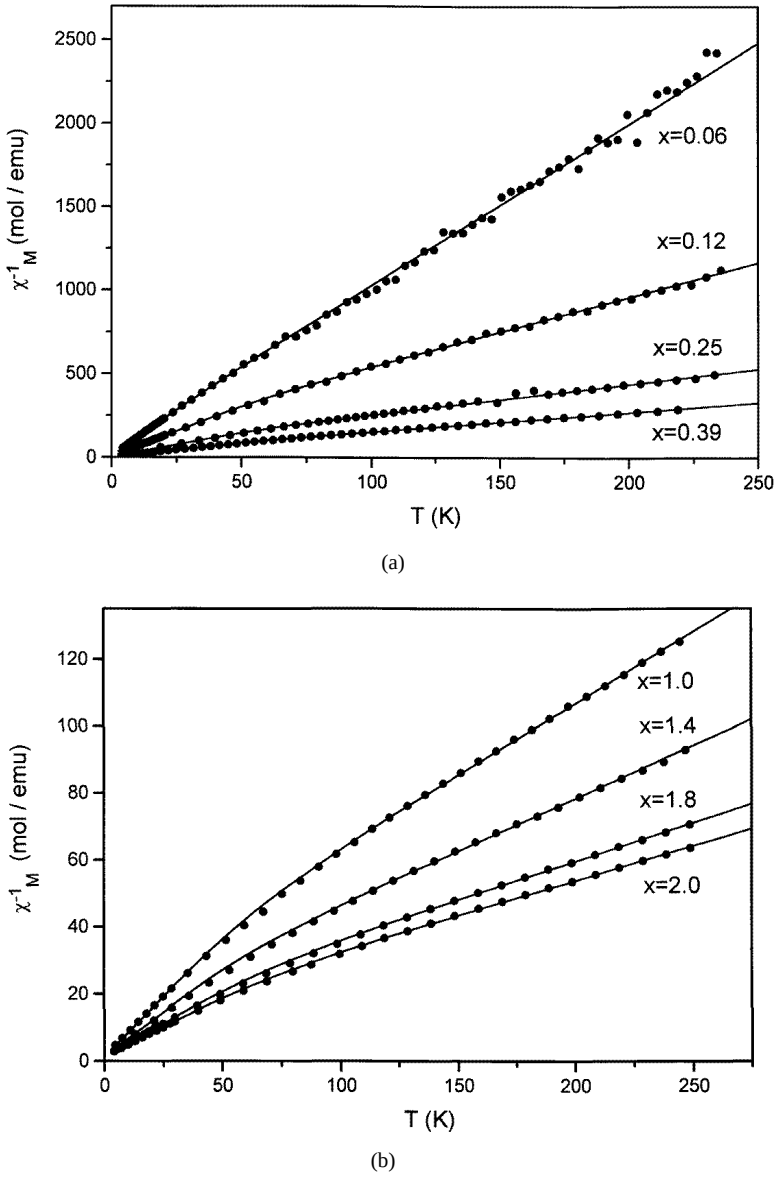

Figure 4. The inverse susceptibilities for $Yb_xY_{2-x}O_3$ samples over the full temperature range. The experimental points are given by the dots, and the calculated curves by the full lines.

constant for the free Yb^{3+} ions, given by the expression $N_{Av}g_J^2\mu_B^2J(J+1)/3k_B = 2.57$ emu K/g-ion. The values obtained for θ versus concentration are shown in figure 5, and one can see that the $\theta(x)$ dependence is linear within the experimental error. This result shows the absence of strong clustering of magnetic Yb^{3+} ions; in this case the number of magnetic neighbours increases linearly with concentration.

For the calculation of the magnetic susceptibility over the whole temperature region, the Curie constant C_M is no longer temperature independent, because the higher Kramer's doublets must be included. In the temperature region of the measurements it was sufficient

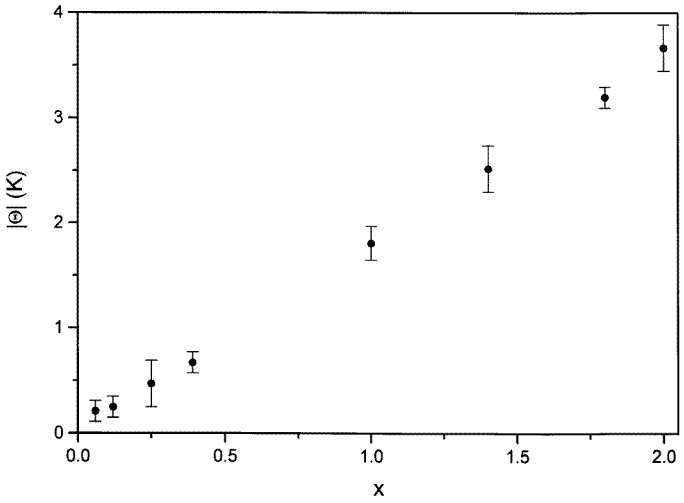

Figure 5. The absolute values of the Curie–Weiss paramagnetic temperatures θ obtained from the low-temperature region ($T < 30$ K). Note that all of the θ-values are negative.

to include only the first excited doublet, and thus now C_M can be expressed by the following equation:

$$C_M = \frac{x g_J^2 \mu_B^2 N_{Av}}{k_B} \frac{M_{1eff}^2 + M_{2eff}^2 \mathrm{e}^{-\Delta W/k_B T}}{1 + \mathrm{e}^{-\Delta W/k_B T}} \tag{5}$$

where M_{1eff} and M_{2eff} are the effective magnetic quantum numbers of the Kramer's doublets, and ΔW is the energy gap between them. M_{1eff} was taken from the low-temperature region, and the remaining two parameters M_{2eff} and ΔW were fitted. The results for M_{2eff} and ΔW are listed in table 3.

5. Conclusion

All of the $Yb_xY_{2-x}O_3$ solid solutions, except $Yb_{0.06}Y_{1.94}O_3$, are characterized by weak preferential occupation of Yb^{3+} ions in 24d sites. Only in the $Yb_{0.06}Y_{1.94}O_3$ sample do the Yb^{3+} ions, within the experimental error, exclusively occupy 24d positions.

The magnetic moments obtained from the neutron diffraction measurements on the Yb_2O_3 single crystal at 1.25 K are $\mu(24d) = (1.81 \pm 0.06)\mu_B$ and $\mu(8b) = (1.05 \pm 0.06)\mu_B$ [6]. The measurements on the powder gave the magnetic moment for the 24d crystallographic positions as $\mu(24d) = (1.91 \pm 0.08)\mu_B$ [6]. Our result for the magnetic moment of the Yb^{3+} ion in $Yb_{0.06}Y_{1.94}O_3$ (where Yb^{3+} ions approximately fill only 24d crystallographic positions) is $2.00(14)\mu_B$, and this is practically the same as the result obtained from powder neutron measurements [6]. The effective magnetic quantum numbers M_{1eff} of the first Kramer's doublets of Yb^{3+} ions are the same within the experimental error for all concentrations x (table 3). This result is expected as an effect of the action of the weak crystal fields that preserved the same symmetry in all of the samples. A similar conclusion can be drawn for the effective magnetic quantum number M_{2eff} for the second Kramer's doublet, except for the $Yb_{0.06}Y_{1.94}O_3$ and $Yb_{0.12}Y_{1.88}O_3$ samples. The small difference in the M_{2eff}-values for these samples can be explained in terms of the preferential occupation by Yb^{3+} ions of the 24d position.

The energy gap ΔW generally depends on the cation's surroundings, and cation–anion distances. In our case the changes of $\Delta W(x)$ are the consequence of different cation–anion distances. The crystal fields are different for the 24d and 8b positions. Hence, the energy gap obtained from magnetic susceptibility measurements for $x > 0.06$ corresponds to an average crystal field for the 24d and 8b positions. The energy gap $\Delta W/k_B = 80$ K for $x = 0.06$ corresponds to the crystal field for the 24d position.

For pure Yb_2O_3 and for all $Yb_xY_{2-x}O_3$ samples, the Curie–Weiss paramagnetic temperatures $\theta(x)$ obtained from the low-temperature region ($T < 30$ K) are small and negative, and they depend linearly on the concentration x (figure 5). This θ-behaviour is a result of the dominant antiferromagnetic exchange interaction between Yb^{3+} ions. Note that the large negative value $\theta = -90$ K for Yb_2O_3 obtained from the high-temperature susceptibility [7] is a consequence of the crystal-field effects.

Acknowledgments

The authors thank Dr V Kusigerski for helpful suggestions, and Mr I Stanic for technical support during the experiments.

References

[1] Mitric M, Onnerud P, Rodic D, Tellgren R, Szytula A and Napijalo M Lj 1993 *J. Phys. Chem. Solids* **54** 967
[2] Antic B, Onnerud P, Rodic D and Tellgren R 1993 *Powder Diffract.* **8** 216
[3] Antic B, Mitric M and Rodic D 1995 *J. Magn. Magn. Mater.* **145** 349
[4] Rodic D, Antic B and Mitric M 1995 *J. Magn. Magn. Mater.* **140–144** 1181
[5] Marezio M 1966 *Acta Crystallogr.* **20** 723
[6] Moon R M, Koehler W C, Chilo H R and Raubenheimer L J 1968 *Phys. Rev.* **176** 722
[7] Sucksmith W 1932 *Phil. Mag.* **14** 1115
[8] Hacker H Jr, Lin M S and Westrum E F Jr 1965 *Proc. 4th Conf. on Rare Earth Research* ed LeR Eyring (New York: Gordon and Breach) p 93
[9] Wiles D B and Young R A 1981 *J. Appl. Crystallogr.* **14** 149
[10] Smrcok L 1989 *Cryst. Res. Technol.* **24** 607
[11] *International Tables for X-ray Crystallography* 1974 vol IV (Birmingham: Kynoch) pp 100–1
[12] Hovestreydt E 1983 *Acta Crystallogr.* A **39** 268
[13] Shannon R D and Prewitt C T 1969 *Acta Crystallogr.* B **25** 925
[14] Selwood P C 1956 *Magnetochemistry* (New York: Interscience) p 78
[15] Gruber J B, Chirico R D and Westrum E F Jr 1982 *J. Chem. Phys.* **76** 4600
[16] Chang N C, Gruber J B, Leavitt R P and Morrison C A 1982 *J. Chem. Phys.* **76** 3877
[17] Gruber J B, Leavitt R P, Morrison C A and Chang N C 1985 *J. Chem. Phys.* **82** 5373
[18] Justice B H and Westrum E F Jr 1963 *J. Phys. Chem.* **67** 345